11th International Symposium on Magnetic Bearings
August 26-29, Nara, Japan

AN APPROACH TO A 3-POLE ACTIVE MAGNETIC BEARING SYSTEM FED BY A MATRIX CONVERTER

Javier Vadillo, Jose M. Echeverria, Ibon Elosegui and Luis Fontan
Dept. of Electronics and Communications, CEIT and Tecnun (University of Navarra),
San Sebastian, Gipuzkoa 20009, Spain
jvadillo@ceit.es, jmecheverria@ceit.es,ielosegui@ceit.es, fontan@ceit.es

ABSTRACT
This paper presents a MATLAB/Simulink model for a 3-pole radial magnetic bearing system that is fed by a matrix converter (MC). The active magnetic bearings (AMBs) system model that is studied here is shown and tested in [1] using a simplified inverter model, so that the main contribution of this paper lies in the simulation, study and analysis of the AMBs performance under a MC supply. In order to achieve this objective, a more complex inverter model, including the rectifier stage, and a MC model are implemented, analysed and compared in conjunction with the bearings. Results from models described in [1] are taking into consideration in order to verify the new models performance.

INTRODUCTION
In recent years energy storage flywheels have found wide applications in many areas such as uninterruptible power supplies (UPS), systems for power quality in power networks, improvement of the performance in wind generation systems and to avoid electric consumption peaks in high speed railway substations.

Moreover flywheels promise an alternative to chemical batteries for space systems like artificial satellites because of their higher efficiency in terms of energy per mass and volume, and have become an important area of research for use in electric/hybrid vehicles.

Main advantages of this technology are high energy density, long life, 90% depth of discharge and pulse power capability.

Due to high rotation speed, energy flywheel systems use AMBs to provide non-contact suspension, which is necessary to minimize the friction losses and to achieve long life and maintenance free systems.

Most of the magnetic radial bearings use the 8-pole arrangement because the magnetic flux coupling effects are neglected with this structure. However the 8-pole arrangement imposes the use of at least four independent power amplifiers, one for each pair of poles, and has the disadvantage of large energy losses.
In present paper a 3-pole radial magnetic bearing is considered [1]. The 3-pole arrangement has the advantage of lower power losses, inferior number of power amplifiers and much more space for heat dissipation and to place coils and sensors [2, 3].

3-pole radial magnetic bearing system can be powered by means of an ordinary 3-phase bridge inverter [4]. In case of a low cost solution this can be the most efficient design at present; nevertheless new and more optimized power converter families are being developed nowadays. These new converter families can contribute their performance improvements to the operation of the energy storage systems presented here.

One of these, more optimized, power converters is the MC. In general, a MC is a direct AC-AC power converter that consists of an array of n x m bidirectional power switches, so that any output phase can be directly connected to any input phase, at any time [5]. The main characteristics of a MC are [6]: Direct AC-AC polyphase power conversion, inherent bidirectional power flow capability, input/output senoidal waveforms with variable output voltage amplitude and frequency, input power factor control despite the load in the output side and a simple and compact power circuit because of the elimination of bulky and non-fault-tolerant reactive elements. These are the reasons why this topology is being thoroughly studied nowadays, trying to enter the market as an alternative or improved choice to the well

known dc-link voltage source inverters (VSI). MC presents some limitations too. Perhaps, the most important is the voltage transfer ratio limitation, with a maximum value of 0.86 [7]. Besides, the direct connection between output and input causes a great sensibility to grid distortions. This problem, as well as the large number of semiconductor devices in the power stage, the complexity of the modulation algorithms or the correct commutation between the bidirectional switches [8], has been partially or totally overcome in recent years [9, 10].

This paper analyses the feasibility of the utilization of a MC powering a 3-pole AMBs system, which is part of a kinetic energy storage system.

SYSTEM DESCRIPTION

Although this paper analyses simulation models, physical and electrical parameters concerning a real prototype have to be taken into consideration for a future comparison when a MC prototype is finished.

Figure 1a shows the real kinetic energy storage system overview, and the radial magnetic bearing system can be observed in Figure 1b. System described in Figure 1b is that which will be simulated and analysed in conjunction with its control and the MC.

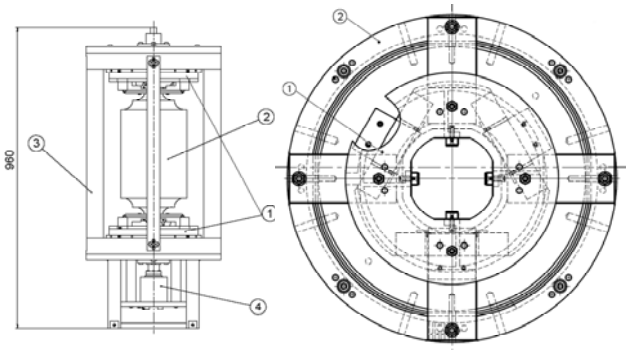

FIGURE 1: a) System overview (1-Radial AMB, 2-Flywheel, 3-Frame, 4-Air turbine) b) 3-Pole Radial Magnetic Bearing (1-Coil, 2-Magnetic core).

Physical implementation includes a 3-phase dc link VSI, with a 125 Vdc bus to power the three coils. It can provide up to 40A in order to get about 800N force. The flywheel weighs 30 kg and it uses an air-turbine to move the shaft, but a reluctance motor is considered to be connected to the system in order to reach 10.000rpm when it will work like a generator.

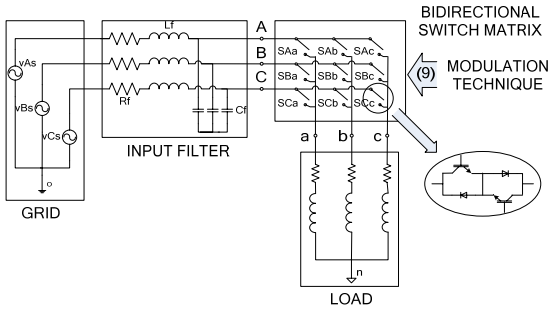

FIGURE 2: Three phase Matrix Converter

MATRIX CONVERTER FUNDAMENTALS

MC consists of an array of bidirectional switches that connects directly the load to the source. The most common studied matrix structure is that formed by nine bidirectional switches in a 3x3 array [11]. A basic structure of the power circuit in a MC is presented in Figure 2. This figure shows the bidirectional switch matrix, including a possible real implementation of the bidirectional switches [12], and an input filter for smoothing source currents.

The converter is completed with the control stage, which generates, and applies in a safe way, the correct control signals to the power switches in order to obtain the desired output voltage and input current waveforms. As far as the model is concerned, the control stage will be represented by the implementation of 9 switching functions (1) for the ideal bidirectional switches in Figure 2.

$$S_{Kj} = \begin{cases} 1, \text{switch } S_{Kj} \text{ closed} \\ 0, \text{switch } S_{Kj} \text{ open} \end{cases} \quad \begin{matrix} K = \{A, B, C\} \\ j = \{a, b, c\} \end{matrix} \qquad (1)$$

The mathematical expressions that represent the basic operation of the MC are obtained applying Kirchhoff's voltage and current laws to the switch array (2, 3):

$$\begin{bmatrix} v_a(t) \\ v_b(t) \\ v_c(t) \end{bmatrix} = \begin{bmatrix} S_{Aa}(t) & S_{Ba}(t) & S_{Ca}(t) \\ S_{Ab}(t) & S_{Bb}(t) & S_{Cb}(t) \\ S_{Ac}(t) & S_{Bc}(t) & S_{Cc}(t) \end{bmatrix} \cdot \begin{bmatrix} v_A(t) \\ v_B(t) \\ v_C(t) \end{bmatrix} \qquad (2)$$

$$\begin{bmatrix} i_A(t) \\ i_B(t) \\ i_C(t) \end{bmatrix} = \begin{bmatrix} S_{Aa}(t) & S_{Ba}(t) & S_{Ca}(t) \\ S_{Ab}(t) & S_{Bb}(t) & S_{Cb}(t) \\ S_{Ac}(t) & S_{Bc}(t) & S_{Cc}(t) \end{bmatrix}^T \cdot \begin{bmatrix} i_a(t) \\ i_b(t) \\ i_c(t) \end{bmatrix} \qquad (3)$$

Where v_a, v_b and v_c are the output phase voltages, and i_A, i_B and i_C represent the input currents to the matrix.

The output voltage is directly constructed switching between the input voltages and the input currents are obtained in the same way from the output ones.

For these equations to be valid, next expression has to be taken into consideration:

$$S_{Aj} + S_{Bj} + S_{Cj} = 1, \quad j = \{a, b, c\} \tag{4}$$

What this expression says is that, at any time, one, and only one switch must be closed in an output branch. If two switches were closed simultaneously, a short circuit would be generated between two input phases. On the other hand, if all the switches in an output branch were open, the load current would be suddenly interrupted and, due to the inductive nature of the load, an over voltage problem would be produced in the converter. This is the reason that makes it necessary to implement commutation methods [13] that allow the current to be commutated safely between the different IGBTs within real bidirectional switches.

Matrix Converter Modulation

MC is controlled (modulated) by means of selecting an appropriate set of switching functions (1), in such a way that the output voltages and input currents reach the values chosen by the user or by a reference. Many methods have been reported [6, 9, 14, 15]: Venturini (and optimized), indirect, scalar methods... This paper focuses on the direct space vector modulation (DSVM) method.

Direct Space Vector Modulation Algorithm. DSVM algorithm uses 21 of 27 possible states that can be generated by the matrix of bidirectional switches. These states are presented in Table 1.

Output voltage and input current space vectors form two hexagons that limit any possible reference vectors to be generated by the MC, as can be seen in Figure 3.

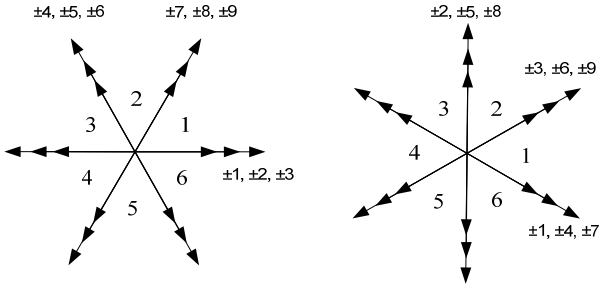

FIGURE 3: Output voltage and input current space vector hexagons.

TABLE 1: Switching states and vectors used in DSVM

MC State		Switches on	$\lvert\vec{v}_o\rvert$	$\angle\vec{v}_o$	$\lvert\vec{i}_i\rvert$	$\angle\vec{i}_i$
ABB	+1	S_{Aa} S_{Bb} S_{Bc}	2/3 v_{AB}	0	2/√3 i_a	-π/6
BAA	-1	S_{Ba} S_{Ab} S_{Ac}	-2/3 v_{AB}	0	-2/√3 i_a	-π/6
BCC	+2	S_{Ba} S_{Cb} S_{Cc}	2/3 v_{BC}	0	2/√3 i_a	π/2
CBB	-2	S_{Ca} S_{Bb} S_{Bc}	-2/3 v_{BC}	0	-2/√3 i_a	π/2
CAA	+3	S_{Ca} S_{Ab} S_{Ac}	2/3 v_{CA}	0	2/√3 i_a	7π/6
ACC	-3	S_{Aa} S_{Cb} S_{Cc}	-2/3 v_{CA}	0	-2/√3 i_a	7π/6
BAB	+4	S_{Ba} S_{Ab} S_{Bc}	2/3 v_{AB}	2π/3	2/√3 i_b	-π/6
ABA	-4	S_{Aa} S_{Bb} S_{Ac}	-2/3 v_{AB}	2π/3	-2/√3 i_b	-π/6
CBC	+5	S_{Ca} S_{Bb} S_{Cc}	2/3 v_{BC}	2π/3	2/√3 i_b	π/2
BCB	-5	S_{Ba} S_{Cb} S_{Bc}	-2/3 v_{BC}	2π/3	-2/√3 i_b	π/2
ACA	+6	S_{Aa} S_{Cb} S_{Ac}	2/3 v_{CA}	2π/3	2/√3 i_b	7π/6
CAC	-6	S_{Ca} S_{Ab} S_{Cc}	-2/3 v_{CA}	2π/3	-2/√3 i_b	7π/6
BBA	+7	S_{Ba} S_{Bb} S_{Ac}	2/3 v_{AB}	4π/3	2/√3 i_c	-π/6
AAB	-7	S_{Aa} S_{Ab} S_{Bc}	-2/3 v_{AB}	4π/3	-2/√3 i_c	-π/6
CCB	+8	S_{Ca} S_{Cb} S_{Bc}	2/3 v_{BC}	4π/3	2/√3 i_c	π/2
BBC	-8	S_{Ba} S_{Bb} S_{Cc}	-2/3 v_{BC}	4π/3	-2/√3 i_c	π/2
AAC	+9	S_{Aa} S_{Ab} S_{Cc}	2/3 v_{CA}	4π/3	2/√3 i_c	7π/6
CCA	-9	S_{Ca} S_{Cb} S_{Ac}	-2/3 v_{CA}	4π/3	-2/√3 i_c	7π/6
AAA	0_1	S_{Aa} S_{Ab} S_{Ac}	0	-	0	-
BBB	0_2	S_{Ba} S_{Bb} S_{Bc}	0	-	0	-
CCC	0_3	S_{Ca} S_{Cb} S_{Cc}	0	-	0	-

Output voltage reference, v_o, as can be observed in Figure 4, is split along the nearest active vectors within its sector. Furthermore, input current reference vector, i_{in}, direction is imposed to be the same as the input voltage vector one. According to this combination of input current and output voltage reference vectors location, Table 2 presents the group of four active vectors that have to be applied on each commutation period, T_s, so that it is possible to modulate the input current and the output voltage at the same time.

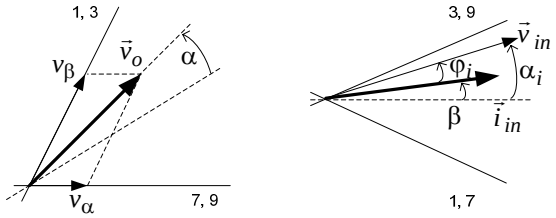

FIGURE 4: Output voltage and input current reference space vectors

Duty cycles expressions for each MC state to be applied along T_s according to Table 2, are obtained in (5) from output voltage and input current reference space vectors location (sector and phase angle measured from the bisecting line within the corresponding sector). The modulation period is completed using zero vectors.

TABLE 2: Active vectors groups for each T_s

$i_{1\,ref}$ vector location	Output voltage reference vector Sector											
	1 or 4				2 or 5				3 or 6			
1 or 4	9	7	3	1	6	4	9	7	3	1	6	4
2 or 5	8	9	2	3	5	6	8	9	2	3	5	6
3 or 6	7	8	1	2	4	5	7	8	1	2	4	5
	I	II	III	IV	I	II	III	IV	I	II	III	IV

$$
\begin{aligned}
d_I &= (-1)^{K_v+K_i}\,\frac{2}{\sqrt{3}}\,q\,\frac{\cos(\alpha-\pi/3)\cos(\beta-\pi/3)}{\cos\varphi_i}\\
d_{II} &= (-1)^{K_v+K_i+1}\,\frac{2}{\sqrt{3}}\,q\,\frac{\cos(\alpha-\pi/3)\cos(\beta+\pi/3)}{\cos\varphi_i}\\
d_{III} &= (-1)^{K_v+K_i+1}\,\frac{2}{\sqrt{3}}\,q\,\frac{\cos(\alpha+\pi/3)\cos(\beta-\pi/3)}{\cos\varphi_i}\\
d_{IV} &= (-1)^{K_v+K_i}\,\frac{2}{\sqrt{3}}\,q\,\frac{\cos(\alpha+\pi/3)\cos(\beta+\pi/3)}{\cos\varphi_i}\\
d_o &= 1-d_I-d_{II}-d_{III}-d_{IV}
\end{aligned}
\qquad (5)
$$

Where K_v and K_i are the sectors where reference vectors are located, q is the voltage ratio, α and β are the phase angle within the sectors and φ_i is the displacement angle between input voltage and current space vectors.

Switching Strategies. Switching strategies deal with the switching configuration sequence, that is, the order in which the active and zero vectors are applied along the commutation period. The three possible zero configurations that can be applied produce two degrees of freedom in order to complete the zero state switching time. In this paper the asymmetrical space vector modulation (ASVM) [10] is implemented.

The ASVM uses only one of the three zero configurations in the middle of the sequence so that minimum switch commutations are achieved between one MC state and the next one. Using this technique the switching commutations are up to 8 for each commutation period and this way switching losses are minimized.

For example, considering both output voltage and input current reference vectors located in sector 1 within their respective hexagons, it can be seen that this is the only possible double-sided sequence that can be generated for ASVM technique:

ASVM

ACC-AAC-AAA-AAB-ABB | ABB-AAB-AAA-AAC-ACC

The zero MC state to be applied is defined in terms of the reference vectors location, as it can be seen in Table 3.

TABLE 3: Zero Configurations for ASVM

$\vec{i}_{iref}$	$\vec{v}_{oref}$
	1, 2, 3, 4, 5 or 6
1 or 4	AAA
2 or 5	CCC
3 or 6	BBB

SYSTEM MODELLING

Figure 5a shows a general block diagram for the whole system to be modelled and 5b its corresponding Simulink implementation. The three main parts of the system can be observed in these diagrams; the 3-pole AMBs model, the control scheme and the power converter, which is in charge of the supply of the correct voltages to the bearings from the references generated by the control stage.

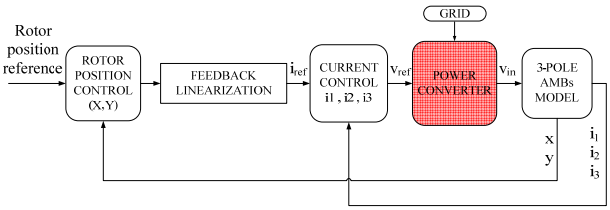

FIGURE 5a: System modelling block diagram

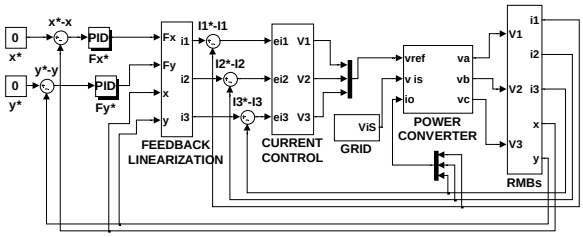

FIGURE 5b: Simulink model of the system

The 3-pole AMBs model is described in detail in [1]. Basically, the model works in order to obtain the right currents in the coils, that is, the correct forces on the rotor, so that the position references are achieved. These currents are obtained from bearing voltages, which are generated by the power converter for a given set of input voltage references that are obtained from the current control. Equations that describe the model of the bearings are those related to an RL load, but with

inductances that are calculated in terms of a non-constant in time air gap that depends on the rotor position (x,y), which are defined in Figure 6.

A radial force disturbance that represents the centrifugal force acting on the rotor because of the angular speed is applied to the AMBs model. This disturbance is simulated as a sine which is subtracted from x component of the force to be applied in the coils, and a cosine that is applied to the y component. Both disturbance components are simulated increasing their frequency and amplitude in terms of the angular speed for the start up process, and maintaining these variables for the permanent operation.

Due to the nonlinearity of the relationship between forces that have to be applied in the load, and the magnetic fluxes generated by the coils, a feedback linearization has to be used. This way a simple PID control can be applied for the position control.

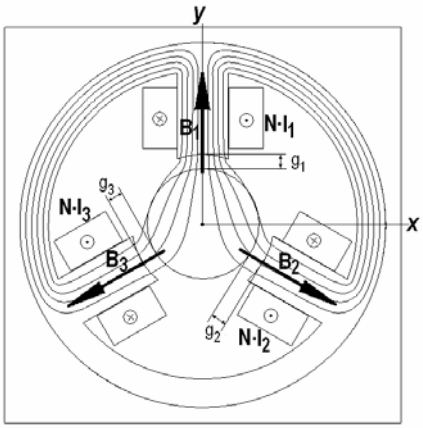

FIGURE 6: Magnetic circuit of the 3-pole AMB

Power Converter Modelling

As it was described before, this paper focuses on the power converter that has to provide the correct voltages to the bearings model. A simple model for a VSI inverter is used in [1] in order to test the control and the AMBs model. This model outputs two different constant voltages, V_{bus} or $-V_{bus}$ in terms of a comparison between a triangular wave and the reference voltages.

Voltage Source Inverter Model. In order to analyze the currents in the grid side of the converter, a more comprehensive model has to be implemented. Rectifier diode-bridge, IGBT-bridge or the DC bus models are implemented using the SimPowerSystems toolbox in Simulink, as it can be seen in Figure 7. Power devices are considered almost ideal in this first approach. Observable variables in the simplified model are proved to be absolutely consistent with this less simplified model.

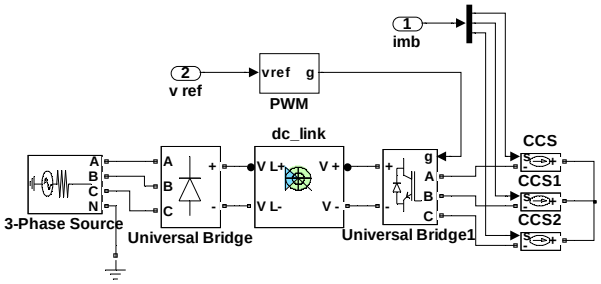

FIGURE 7: VSI Simulink model

Matrix Converter Model. Simulink model for the MC can be seen in Figure 8. The MC array is modelled using ideal (bidirectional) switches. This way, no commutation strategy is necessary to be simulated in order to achieve a safe commutation between bidirectional switches. These switches are activated by nine control signals that are generated by the DSVM algorithm. In order to compare input currents between models, and for the simplicity of the whole model, no input filter has been added, although its utilization with a MC is imperative in order to smooth the obtained currents.

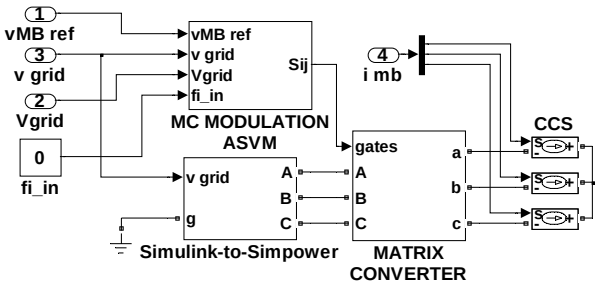

FIGURE 8: Matrix Converter Simulink model

DSVM algorithm model is shown in Figure 9. First, the associated voltage space vector for the voltages to be applied to the AMBs (output of the converter) has to be calculated using (6). The input current reference space vector is calculated from the grid voltages, imposing an input displacement factor equal to 0. Then duty cycles for active and zero vectors are calculated according to (5). Afterwards, active and zero vectors are organized within each commutation period according to Tables 2 and 3. Finally the MC nine control signals are obtained from a list that includes all the MC states and their corresponding switching functions.

$$\vec{x} = \frac{2}{3}\left(x_a + x_b \cdot e^{j\frac{2\pi}{3}} + x_c \cdot e^{j\frac{4\pi}{3}} \right) \quad (6)$$

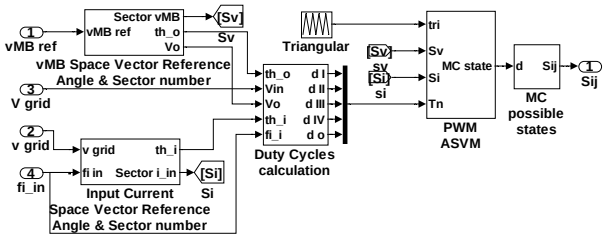

FIGURE 9: Modulation algorithm Simulink model

RESULTS AND DISCUSSION

Comparison between simulations for the power converter models described above is presented next. Input voltage to the power converter is set to $90V_{rms\ L\text{-}L}$, as in the real flywheel prototype. The commutation frequency for PWM in the VSI and for the DSVM in the MC is chosen to be 10 KHz.

Simulations are carried out as follows. Initial condition for the rotor position is: x_0=1e-3m, y_0=-1e-3m. No radial disturbance is applied until t=0.1s, so flywheel is taken into equilibrium before starting to rotate. In t=0.1s disturbance is activated. Its frequency is increased until 167Hz, that is, until 10020rpm, when t=0.3s is reached. From t=0.3s disturbance is maintained in frequency and amplitude.

Figure 10 shows the currents in the 3-pole AMB system obtained from the VSI and from the MC.

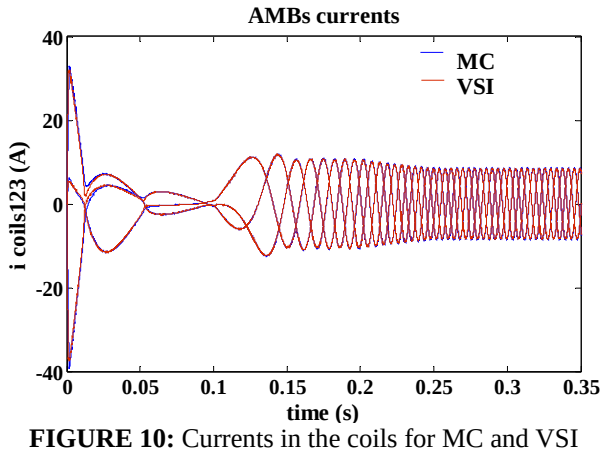

FIGURE 10: Currents in the coils for MC and VSI

As a consequence of these currents, x and y position magnitudes of the rotor are obtained in Figures 11 and 12. The flywheel starts its operation in a disequilibrium position (x=1e-3m and y=-1e-3m). It can be seen that the rotor is nearly stabilized by t=0.1s. It is then when the disturbance starts. Control parameters can be optimized in order to optimize transient responses.

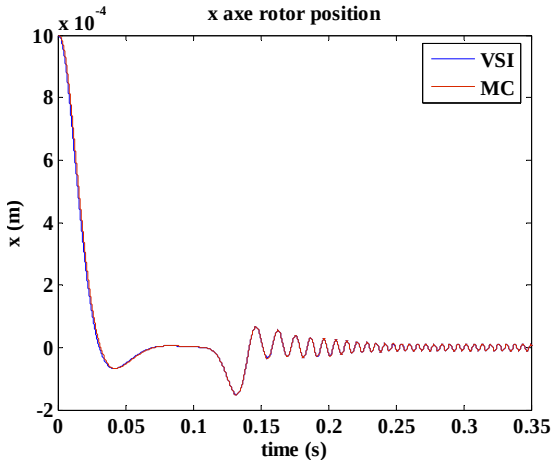

FIGURE 11: Flywheel position component x

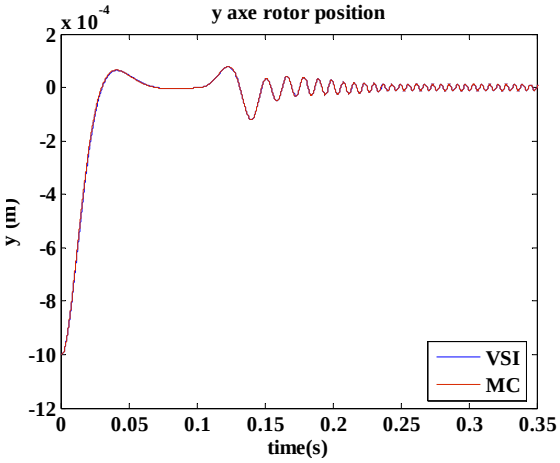

FIGURE 12: Flywheel position component y

Due to the different power converter used in order to feed the 3-pole AMBs system, different waveforms for the grid currents are obtained. Source current for VSI can be seen in Figure 13, and the MC input current can be observed in Figure 14.

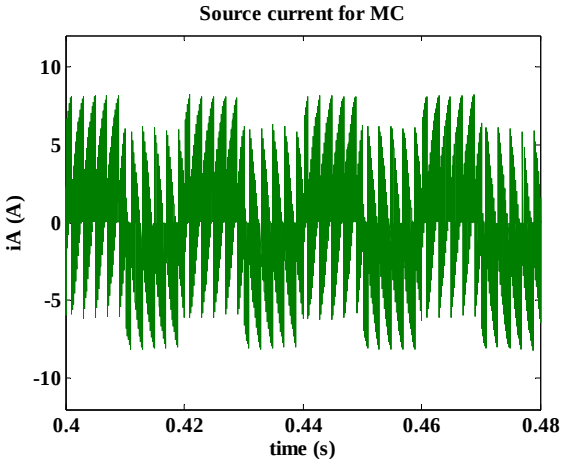

FIGURE 13: Input current for the MC

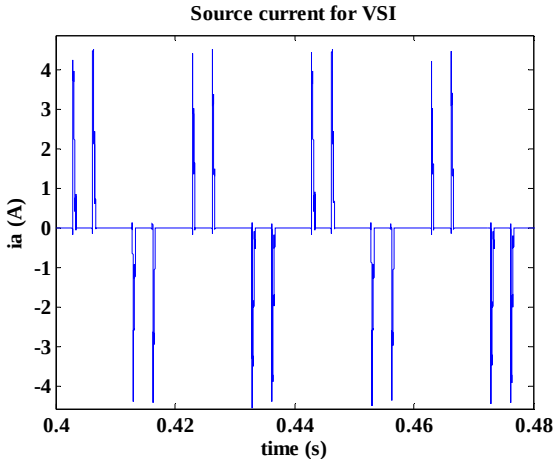

FIGURE 14: Input current for the VSI

FFT for currents presented in Figures 13 and 14 are shown in Figures 15 and 16. A zoom for both figures considering frequencies below 15 KHz is shown in Figure 17.

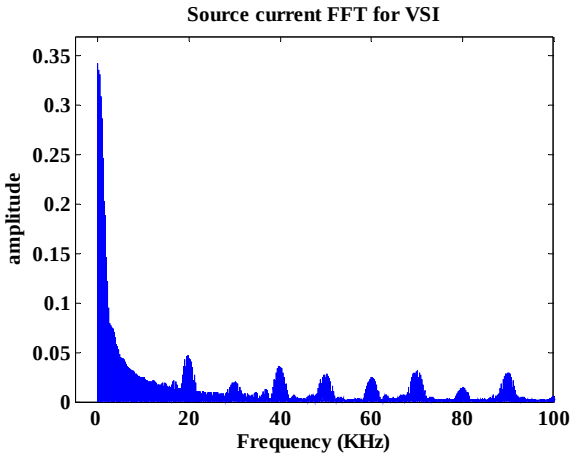

FIGURE 15: Input current FFT for the VSI

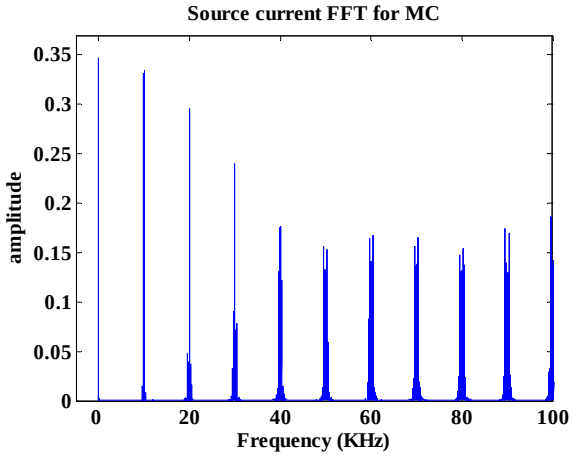

FIGURE 16: Input current FFT for the MC

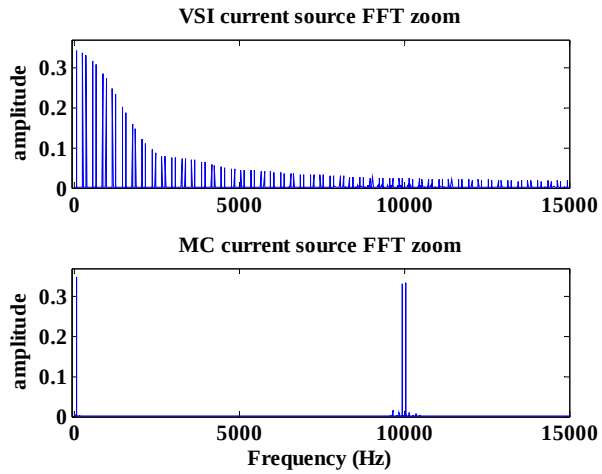

FIGURE 17: Input current FFT zoom for VSI and MC

Finally, Figure 18 presents input voltage (rescaled) and the filtered source current for the MC in phase A, using a cut off frequency of 1KHz.

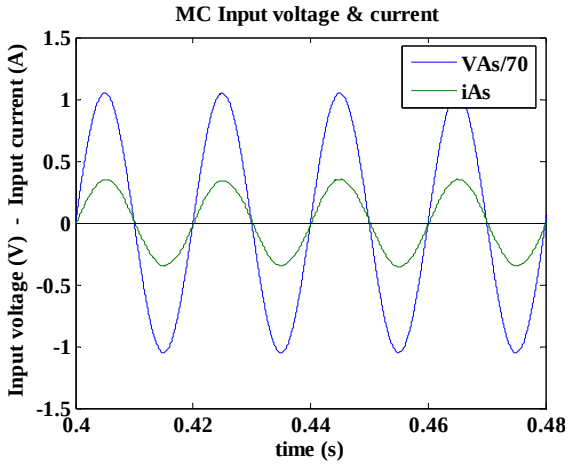

FIGURE 18: MC input current and voltage (rescaled)

Figures 10, 11, and 12 show clearly that both VSI and MC models work just in the same way as far as the AMBs system model is concerned. Equivalent currents, and then, the same position controls are obtained using both power converters. This way, the flywheel is equally controlled using either the MC or the VSI. It is able to supply voltages that are built in a very different way, to the AMBs model.

Main differences are presented for the current in the input side of the converters. The MC input current is built commutating directly between the output currents, because its direct link between the input and the output. Figure 15 and 16 show the FFT for both input currents. Although commutation frequency harmonics are quite higher in the MC current, it can be seen that components between fundamental and commutation

frequencies are negligible. This range of frequencies is just the same where VSI input current harmonics are much higher. This fact is clearly presented in a zoom of the FFTs in Figure 17.

Besides, the MC modulation algorithm model, the DSVM, is proved to work just as it was configured to do. Without an input filter, the input zero displacement angle reference is totally achieved, as it can be observed in Figure 18. At the same time, it provides the referenced output voltages to be applied to the AMBs model.

CONCLUSIONS

Taking into consideration the results presented above, the feasibility of the MC model in conjunction with the AMBs system model is proved. No differences are appreciated in the control of the flywheel variables in terms of the power converter.

FFT analysis shows that input filter design is much easier, more effective and cheaper to be implemented for the MC. The relationship between the whole system and the grid is clearly improved. This important advantage, as well as the robustness and the flexibility of the MC in contrast to the VSI, makes it a new solution to be considered in the future for these kind of power applications.

ACKNOWLEDGE

Javier Vadillo's contract is funded by the Ministry of Science and Innovation of Spain within the framework of the Torres Quevedo Programme, and co-funded by the European Social Fund.

REFERENCES

1. Cantero, D., Mihai, G., Martin, F., Vadillo, J. and Fontan, L., PD Control and Sliding Mode Control Using Feedback Linearization for 3-pole Radial Magnetic Bearings of an Energy Storage Flywheel, Proc. of the 10th Int. Symp. on Magnetic Bearings, Martigny, Switzerland, Aug. 21-23, 2006.

2. Chen, S.L. and Hsu, C.T., Optimal design of a Three-Pole Active Magnetic Bearing, IEEE Transactions on Magnetics, vol. 38, issue 5, Sept. 2002, pp. 3458-3466.

3. Hsu, C.T. and Chen, S.L., Nonlinear Control of a 3-Pole Active Magnetic Bearing System, Automatica, vol. 39, issue 2, Feb. 2003, pp. 291-298.

4. Hoffman, W., Behaviour and Control of an Inverter-Fed Three-Pole Active Radial Magnetic Bearing, Proc. of the Int. Symp. on Industrial Electronics, Rio de Janeiro, Brasil, Jun. 9-11, 2003.

5. Venturini, M. and Alesina, A. Generalised transformer: A new bidirectional, sinusoidal waveform frequency converter with continuously adjustable input power factor, Proc. of the Power Electronics Specialists Conference, Atlanta, USA, Jun. 1980.

6. Wheeler, P. W., Rodriguez, J., Clare, J. C., Empringham, L. and Weinstein, A., Matrix converters: A technology review, IEEE Transactions on Industrial Electronics, vol. 49, issue 2, Apr. 2002, pp. 276-288.

7. Alesina, A. and Venturini, M. G. B., Analysis and design of optimum-amplitude nine-switch direct AC-AC converters, IEEE Transactions on Power Electronics, vol. 4, issue 1, Jan 1989, pp. 101-112.

8. Wheeler, P. W., Clare, J. C., Empringham, L., Bland, M. and Kerris, K. G., Matrix converters, IEEE Industry Applications Magazine, vol. 10, issue 1, Jan-Feb 2004, pp. 59-65.

9. Casadei, D., Serra, G., Tani, A. and Zarri, L., Matrix converter modulation strategies: A new general approach based on space-vector representation of the switch state, IEEE Transactions on Industrial Electronics, vol. 49, issue 2, Apr. 2002, pp. 370-381.

10. Casadei, D., Serra, G., Tani, A., Trentin, A. and Zarri, L., Theoretical and experimental investigation on the stability of matrix converters, IEEE Transactions on Industrial Electronics, vol. 52, issue 5, Oct. 2005, pp. 1409-1419.

11. Klumpner, C., Nielsen, P., Boldea, I. and Blaabjerg, F., A new matrix converter motor (MCM) for industry applications, IEEE Transactions on Industrial Electronics, vol. 49, issue 2, Apr. 2002, pp. 325-335.

12. Bland, M.J., Wheeler, P.W., Clare, J.C. and Empringham, L., Comparison of bi-directional switch components for direct AC-AC converters, Proc. of the 35th Power Electronics Specialists Conference, Aachen, Germany, Jun. 20-25, 2004.

13. Mahlein, J., Igney, J., Weigold, J., Braun, M. and Simon, O., Matrix converter commutation strategies with and without explicit input voltage sign measurement, IEEE Transactions on Industrial Electronics vol., 49, issue 2, Apr. 2002, pp. 407-414.

14. CHA, H.J., Analysis and design of matrix converters for adjustable speed drives and distributed power sources. Doctoral dissertation, Texas, USA, Texas A&M, 2004.

15. Huber, L. and Borojevic, D., Space vector modulated three-phase to three-phase matrix converter with input power factor correction, IEEE Transactions on Industry Applications, vol. 31, issue 6, Nov-Dic. 1995, pp. 1234-1246.